

UC Riverside

UC Riverside Previously Published Works

Title

The 5-Ketofructose Reductase of *Gluconobacter* sp. Strain CHM43 Is a Novel Class in the Shikimate Dehydrogenase Family

Permalink

<https://escholarship.org/uc/item/6sw584xn>

Journal

Journal of Bacteriology, 203(19)

ISSN

0021-9193

Authors

Nguyen, Thuy Minh

Goto, Masaru

Noda, Shohei

et al.

Publication Date

2021-09-08



DOI

10.1128/jb.00558-20

Peer reviewed



The 5-Ketofructose Reductase of *Gluconobacter* sp. Strain CHM43 Is a Novel Class in the Shikimate Dehydrogenase Family

Thuy Minh Nguyen,^a Masaru Goto,^b Shohei Noda,^b  Minenosuke Matsutani,^c Yuki Hodoya,^b Naoya Kataoka,^{a,d,e} Osao Adachi,^a Kazunobu Matsushita,^{a,d,e}  Toshiharu Yakushi^{a,d,e}

^aDivision of Life Science, Graduate School of Science and Technology for Innovation, Yamaguchi University, Yamaguchi, Japan

^bDepartment of Biomolecular Science, Graduate School of Science, Toho University, Chiba, Japan

^cNODAI Genome Research Center, Tokyo University of Agriculture, Tokyo, Japan

^dDepartment of Biological Chemistry, Faculty of Agriculture, Yamaguchi University, Yamaguchi, Japan

^eResearch Center for Thermotolerant Microbial Resources, Yamaguchi University, Yamaguchi, Japan

ABSTRACT *Gluconobacter* sp. strain CHM43 oxidizes mannitol to fructose and then oxidizes fructose to 5-keto-D-fructose (5KF) in the periplasmic space. Since NADPH-dependent 5KF reductase was found in the soluble fraction of *Gluconobacter* spp., 5KF might be transported into the cytoplasm and metabolized. Here, we identified the *GLF_2050* gene as the *kfr* gene encoding 5KF reductase (KFR). A mutant strain devoid of the *kfr* gene showed lower KFR activity and no 5KF consumption. The crystal structure revealed that KFR is similar to NADP⁺-dependent shikimate dehydrogenase (SDH), which catalyzes the reversible NADP⁺-dependent oxidation of shikimate to 3-dehydroshikimate. We found that several amino acid residues in the putative substrate-binding site of KFR were different from those of SDH. Phylogenetic analyses revealed that only a subclass in the SDH family containing KFR conserved such a unique substrate-binding site. We constructed KFR derivatives with amino acid substitutions, including replacement of Asn21 in the substrate-binding site with Ser that is found in SDH. The KFR-N21S derivative showed a strong increase in the K_m value for 5KF but a higher shikimate oxidation activity than wild-type KFR, suggesting that Asn21 is important for 5KF binding. In addition, the conserved catalytic dyad Lys72 and Asp108 were individually substituted for Asn. The K72N and D108N derivatives showed only negligible activities without a dramatic change in the K_m value for 5KF, suggesting a catalytic mechanism similar to that of SDH. With these data taken together, we suggest that KFR is a new member of the SDH family.

IMPORTANCE A limited number of species of acetic acid bacteria, such as *Gluconobacter* sp. strain CHM43, produce 5-ketofructose, a potential low-calorie sweetener, at a high yield. Here, we show that an NADPH-dependent 5-ketofructose reductase (KFR) is involved in 5-ketofructose degradation, and we characterize this enzyme with respect to its structure, phylogeny, and function. The crystal structure of KFR was similar to that of shikimate dehydrogenase, which is functionally crucial in the shikimate pathway in bacteria and plants. Phylogenetic analysis suggested that KFR is positioned in a small subgroup of the shikimate dehydrogenase family. Catalytically important amino acid residues were also conserved, and their relevance was experimentally validated. Thus, we propose KFR as a new member of shikimate dehydrogenase family.

KEYWORDS oxidoreductases, nicotinamide, substrate specificity, metabolism

Mannitol is one of the best compounds to support the growth of *Gluconobacter* spp. (1), members of acetic acid bacteria. *Gluconobacter* sp. strain CHM43 (2) oxidizes mannitol to fructose by a membrane-bound, pyrroloquinoline quinone-dependent glycerol dehydrogenase (3). Fructose is further oxidized to 5-keto-D-fructose (D-threo-2,5-hexodiulose,

Citation Nguyen TM, Goto M, Noda S, Matsutani M, Hodoya Y, Kataoka N, Adachi O, Matsushita K, Yakushi T. 2021. The 5-ketofructose reductase of *Gluconobacter* sp. strain CHM43 is a novel class in the shikimate dehydrogenase family. *J Bacteriol* 203:e00558-20. <https://doi.org/10.1128/JB.00558-20>.

Editor Ann M. Stock, Rutgers University-Robert Wood Johnson Medical School

Copyright © 2021 American Society for Microbiology. All Rights Reserved.

Address correspondence to Masaru Goto, goto@biomol.sci.toho-u.ac.jp, or Toshiharu Yakushi, juji@yamaguchi-u.ac.jp.

Received 7 October 2020

Accepted 17 July 2021

Accepted manuscript posted online 26 July 2021

Published 8 September 2021

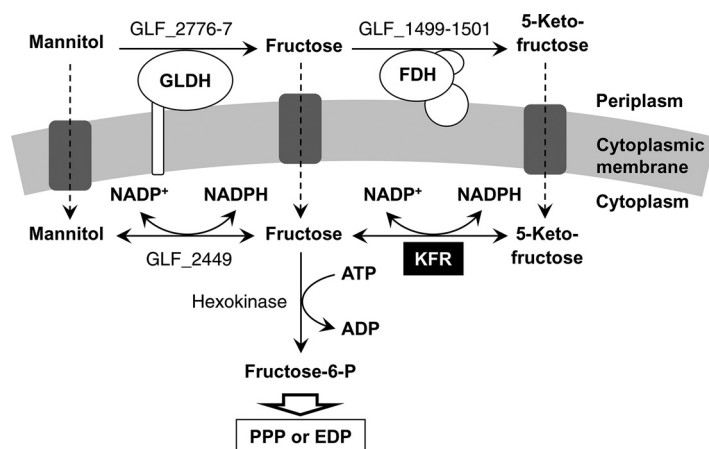


FIG 1 Putative metabolic pathway on mannitol in *Gluconobacter* sp. CHM43. GLDH, pyrroloquinoline quinone-dependent glycerol dehydrogenase; FDH, FAD-dependent fructose dehydrogenase; KFR, 5-ketofructose reductase (GLF_2050); GLF_2449, NADP⁺-dependent mannitol dehydrogenase (68, 69); PPP, pentose phosphate pathway; EDP, Entner Doudoroff pathway.

5KF) by a membrane-bound, flavin adenine dinucleotide (FAD)-dependent fructose dehydrogenase (FDH) (Fig. 1) (4, 5). The electrons formed in these oxidation reactions are transferred to ubiquinone, and ubiquinol is then reoxidized in the respiratory chain by terminal oxidases reducing oxygen to water (6). Periplasmic oxidation is a unique process in several aerobic microorganisms, including the acetic acid bacteria, such as *Gluconobacter* spp., and contributes to the formation of proton motive force across the cytoplasmic membrane and thus to energy metabolism in these microorganisms (7). The oxidative biotransformation of mannitol to 5KF takes place in a nearly stoichiometric manner (8). On the other hand, 5KF metabolism in *Gluconobacter* spp. is not fully understood. Because the CHM43 strain is an efficient 5KF producer (8), we used this strain to examine its 5KF metabolism. Previous *in vitro* studies reported the function of a 5KF reductase (KFR), which catalyzes the reduction of 5KF to fructose with NADPH (9–11). The occurrence of this enzyme suggests the existence of a metabolic pathway for 5KF in *Gluconobacter* cells, in which 5KF first enters the cytoplasm via an unidentified transporter and is then reduced with NADPH to fructose by KFR. Fructose can be phosphorylated to fructose-6-phosphate (Fig. 1) and, after isomerization to glucose-6-phosphate, metabolized via either the pentose phosphate pathway or Entner Doudoroff pathway (1, 12).

5KF is a unique substance produced from mannitol or fructose by *Gluconobacter* strains (8, 13). 5KF is considered a potential low-calorie sweetener, because it cannot be metabolized in the human body (14). It is found for example in wine made from botrytized grapes (15). Thus, 5KF has received attention as a promising natural low-calorie sweetener. The potential economic and human health values of 5KF encouraged studying 5KF metabolism in *Gluconobacter* sp. Here, we identified the *GLF_2050* gene of the CHM43 strain as the gene encoding KFR. The crystal structure of KFR was similar to that of NADP⁺-dependent shikimate dehydrogenase (SDH), and bioinformatics studies suggested that KFR is a member of a specific subclass in the SDH family. Amino acid exchange experiments with KFR identified amino acid residue that is important for substrate binding by KFR.

RESULTS

Identification of *GLF_2050* as the gene for 5KF reductase. We discovered *GLF_2050* as the gene for 5KF reductase (KFR) in the course of a study of NADPH-dependent dihydroxyacetone reductase (NADPH-DHAR) of *Gluconobacter thailandicus* (formerly *Gluconobacter suboxydans*) (16). We found that NADPH-DHAR reduces 5KF at a much higher rate (more than 20 times) than dihydroxyacetone. Thus, we cloned the *GLF_2050* gene from the draft genome of *Gluconobacter* sp. strain CHM43 (17), which is

a homolog of the gene encoding NADPH-DHAR of *G. thailandicus*, to construct recombinant *Escherichia coli* and *Gluconobacter* strains that overexpress GLF_2050. The soluble fractions of the recombinant strains showed higher KFR activity than the control strains that harbor the empty plasmid vectors (see Fig. S1 in the supplemental material). In addition, we constructed a mutant strain of *Gluconobacter* sp. CHM43 in which the *GLF_2050* gene (named *kfr*) was deleted. The KFR activity in the soluble fraction of the Δkfr strain was lower than that of the wild-type strain, 0.36 ± 0.02 and 1.2 ± 0.08 U · (mg protein)⁻¹ in the Δkfr and wild type, respectively. These results indicate that the *GLF_2050* gene encodes KFR, even though an other gene(s) coding for proteins with some KFR activity appears to be present in the CHM43 genome. Schweiger et al. reported that *Gluconobacter oxydans* strain 621H possesses two stereospecific NADPH-dependent ketone reductases, GOX0644 (locus tag number) and GOX1615 (18). Recently, Schiessl et al. reported that the GOX1432 and GOX0644 proteins of *G. oxydans* 621H showed NADPH-dependent KFR activity, the reaction products of which are D-fructose and L-sorbose, respectively (19). Genes homologous to GOX0644, GOX1615, and GOX1432 were found in the CHM43 genome, *GLF_2244*, *GLF_2040*, and *GLF_2249*, respectively. Chen et al. also reported the presence of six NADPH-dependent ketone reductases in *G. oxydans* 621H, including GOX0525 (GLF_2568), GOX1598 (GLF_0138), GOX1462 (GLF_2417), and GOX0290 (GLF_0357) (20). The homologous proteins in the CHM43 strain might contribute the remaining KFR activity measured in the Δkfr derivative (Fig. S1).

Physiological role of KFR in 5KF metabolism. We examined the physiological role of KFR in fructose metabolism of *Gluconobacter* sp. strain CHM43 by analyzing the Δkfr strain. The complemented Δkfr strain was also constructed by introducing a plasmid carrying the *kfr* gene. The wild type, strain Δkfr , and complemented Δkfr mutant ($\Delta kfr/kfr^+$) were cultivated on fructose medium for 10 days to test their ability to consume 5KF (Fig. 2). The periplasmic oxidation system oxidizes fructose to 5KF (Fig. 1). All three tested strains had completely consumed fructose at 3 days and produced 5KF with high efficiency (greater than 75% molar yields). The wild-type strain showed diauxic growth; two growth phases were observed before and after fructose was exhausted (Fig. 2AB). The wild-type strain gradually consumed 5KF and kept the cell growth in the second growth phase. Acetic acid production as a final metabolite (17, 21) was also diphasic, which seems to be related to cell growth (Fig. 2C). The Δkfr mutant showed repressed growth in the second phase, which seemed to be due to inhibited 5KF consumption consistent with no increases in acetic acid production in the second phase (Fig. 2). The repressed growth, decreased 5KF consumption, and acetic acid production were alleviated in the complemented mutant. All if this taken together, we concluded that the *kfr* gene codes for the physiologically relevant KFR.

Characterization of KFR. KFR was purified from the recombinant *Gluconobacter* sp. strain CHM43 harboring pNMT72 (*kfr*⁺) to characterize its biochemical properties and its crystal structure (Fig. S2). We attempted overexpression of KFR in *E. coli*, but the activity was much lower than that of the recombinant *Gluconobacter* strain that overexpresses KFR (Fig. S1). Although we did not carefully characterize these issues, codon preference and protein folding in the *Gluconobacter* cell would be suitable for KFR. As summarized in Table 1, KFR of *Gluconobacter* sp. strain CHM43 showed characteristics similar to those of *Gluconobacter cerinus* NBRC3267 (formerly IFO3267) reported previously (10). The KFR activity was much higher for the reduction of 5KF with NADPH than the reverse reaction, D-fructose oxidation with NADP⁺. The optimum pH and the Michaelis constant for 5KF were similar to those of the KFR of other *Gluconobacter* spp. in previous reports (10, 11, 22). We determined the molecular mass of KFR in solution to be 71 kDa by gel filtration column chromatography, suggesting a dimer of approximately 30-kDa protomers.

Structural overview of *Gluconobacter* 5KF reductase. We determined the crystal structures of the ligand-free KFR and the NADPH-bound KFR. The whole structure of the ligand-free KFR and KFR-NADPH complex was modeled using CCP4 and COOT (23, 24). The overall structure of the KFR-NADPH complex (Fig. 3A) showed a dimer with each

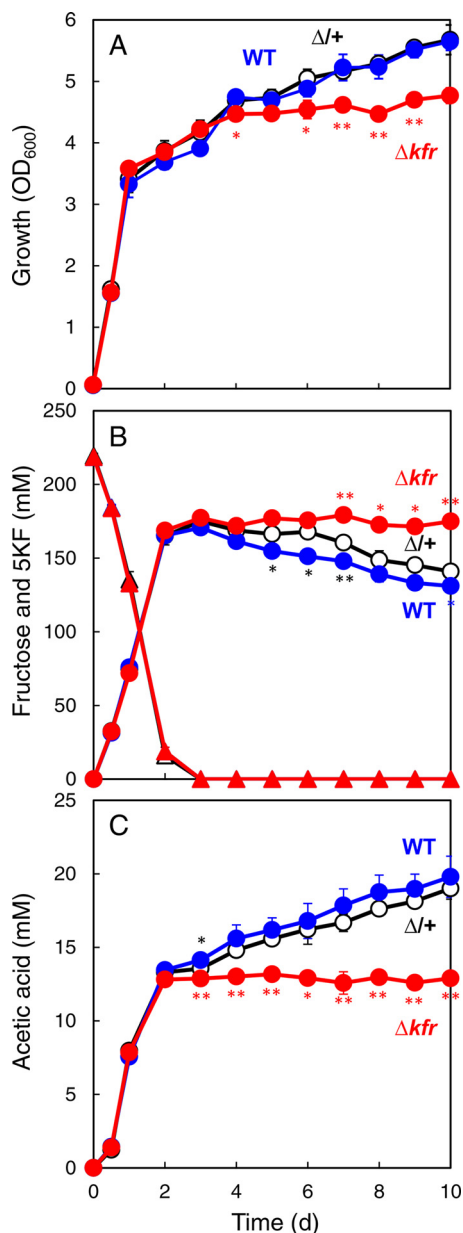


FIG 2 Growth on fructose and concentrations of fructose, 5KF, and acetic acid in the culture medium. The wild-type strain harboring pCM62 (WT), the Δkfr strain harboring pCM62 (Δkfr), and the Δkfr strain harboring p9KX6264 ($\Delta/+$) were precultivated in 2-ml ΔP medium at 30°C with shaking at 120 rpm overnight. Then 1 ml of preculture was inoculated in 100 ml of fructose medium in a 500-ml Erlenmeyer flask, and the cultivation was done at 30°C with shaking at 200 rpm. Samples were taken periodically to measure the OD₆₀₀ (A) and to determine fructose (triangles in panel B), 5KF (circles in panel B), and acetic acid (C) concentrations. Evaporation factors were also determined as described in Materials and Methods to modify the OD₆₀₀ value and the concentrations of fructose, 5KF, and acetic acid. The mean values of triplicate cultivation were plotted, and the error bars represent the standard deviation. Red and black asterisks indicate *P* values between the wild-type and Δkfr strains and between the wild-type and complementary ($\Delta/+$) strains, respectively, using Student's *t* test. *, *P* < 0.05; **, *P* < 0.01.

protomer containing cofactor-binding and substrate-binding domains (Fig. 3B). Thus, it is suggested that the two active sites in the dimer are involved in catalysis. Interprotomer interactions in the structure were analyzed using the PISA service (25) at the European Bioinformatics Institute. There are two KFR molecules in the asymmetric unit. The buried surface between molecules A and B is about 1,213 Å². Analysis of protein interfaces suggests that the homodimer of molecules A and B with the free energy change of the

TABLE 1 Properties of KFRs of *Gluconobacter* spp.

Property	Data from:	
	This study	Avigad et al. (10)
Optimum pH		
5KF reduction (pH)	7.5	7.4
D-Fructose oxidation (pH)	10	NI ^a
Coenzyme specificity	NADPH	NADPH
Sp act [U·(mg protein) ⁻¹]		
5KF reduction	440 ± 30	627
D-Fructose oxidation	1.7 ± 0.02	0.44 ^b
L-Sorbose oxidation	ND ^c	0.31 ^b
Product of 5KF reduction	D-fructose	D-fructose
Kinetic constants		
<i>K_m</i> for 5KF (mM)	4.2 ± 0.4	4.5
<i>V_{max}</i> for 5KF [U·(mg protein) ⁻¹]	920 ± 20	NI
<i>K_m</i> for D-fructose (mM)	8.5 ± 0.6	70
<i>V_{max}</i> for D-fructose [U·(mg protein) ⁻¹]	12 ± 0.2	NI
Molecular mass ^d	71 kDa	NI

^aNI, no information.^bEnzyme assay at pH 7.4.^cND, not detected.^dGel filtration.

intermolecule contact (ΔG^{int}) value of -15.7 kcal/mol is stable in solution. The substrate-binding domains of the two protomers were shown to face to each other in the dimer. Also, one molecule of NADPH binds to the cofactor-binding domain of each subunit. In the KFR-NADPH complex the residues interacting with NADPH through a hydrogen bond or salt bridge were Ala132, Gly134, Ala135, Asn155, Arg156, and Asp157 (Fig. S3). Other residues with close proximity to the cofactor include Gly133, Lys160, Ser199, Val255, Gly248, and Leu252, which are shown to be important for cofactor recognition.

The difference in the distance between the C- α carbons of the main chains of the superposed amino acid residues of the protomer of the ligand-free KFR onto the KFR-NADPH complex was calculated using SUPERPOSE (26) of CCP4i. The average distance between the C- α carbons was 0.42 Å, and its root mean square deviation (RMSD) was 0.46 Å, which shows that the two conformations are very similar (data not shown). Therefore, it was revealed that KFR showed few conformational changes associated with NADPH binding. In addition, the largest distance of 1.68 Å was found between the C- α carbons of the Ser182 residue, which is presumably caused by the movement of the side chain of the Arg156 residue associated with the binding of the adenine ring of NADPH.

Prediction of substrate-binding site in 5KF reductase. We attempted to understand the substrate binding in KFR by comparing the structure of apo-form KFR with the substrate-bound form of a homologous protein. To identify the closest structural relatives to KFR, the PDBefold program was used, and the top hit was for *Escherichia coli* NADP⁺-dependent shikimate dehydrogenase (SDH), with a Z-score of 17.4 based on 264 aligned C-alpha atoms with an RMSD of 1.5 Å (PDB entry 1V12). The top 10 hits were all SDHs from various species, followed by quinate dehydrogenase. Because of the highest similarity to the SDH-shikimate complex, we used the structure of the ternary complex of SDH from *Thermus thermophilus* with bound shikimate and NADPH to examine the substrate binding in KFR. The substrate-binding site in *Thermus* SDH is composed of nine amino acid residues—Ser14, Ser16, Asn58, Thr60, Lys64, Asn85, Asp100, Tyr207, and Gln235 (Fig. 4). According to the structural comparison between the two enzymes, a putative substrate-binding site in KFR was predicted, where Asn58, Lys64, Asn85, Asp100, and Gln235 of SDH corresponded to Asn66, Lys72, Asn93, Asp108, and Gln255 in KFR.

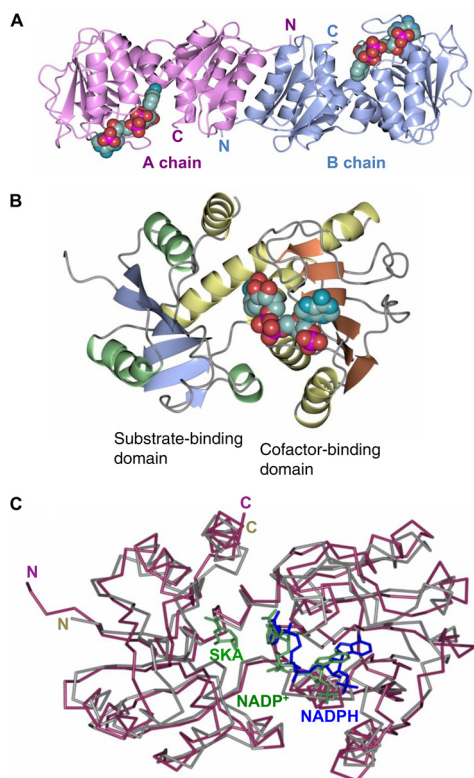


FIG 3 Crystal structure of KFR. (A) Overall structure of NADPH-bound KFR dimer; chains A (pink) and B (blue) in the ribbon model with NADPH in the space-filling model. N, N terminus; C, C terminus. (B) Subunit structure of the 5 KFR-NADPH complex. (C) Superimposed image of the NADPH-KFR complex of *Gluconobacter* sp. CHM43 (purple) and tripartite complex of shikimate, NADPH, and SDH of *Thermus thermophilus* HB8 (37) (gray). NADPH and shikimate are in blue and green, respectively.

Residues Ser14, Ser16, Thr60, and Tyr207 of SDH were different from those in KFR—Asn21, Thr23, Ser68, and Pro227, respectively (Fig. 4). Since Ser14, Ser16, and Tyr207 of SDH interact with the carboxyl group of shikimate, which is absent in 5KF, the residues Asn21, Thr23, and Pro227 in KFR may account for the substrate specificity of KFR, enabling the binding of 5KF and disabling the binding of shikimate. In particular, Asn21

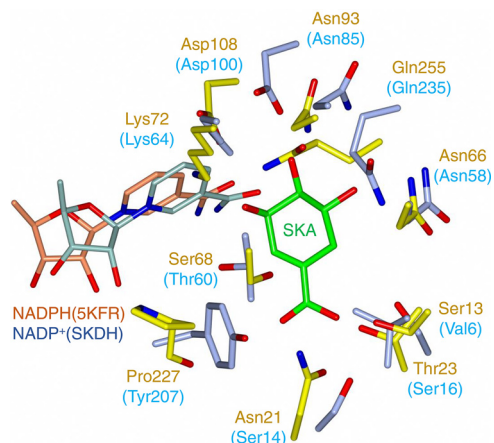


FIG 4 Superimposed image of the substrate-binding site of tripartite NADPH-shikimate-SDH complex and the corresponding site of the NADPH-KFR complex. The substrate-binding site of SDH of *Thermus thermophilus* HB8 (37) complexed with shikimate (green) and NADP⁺ (blue) includes 9 residues shown in light blue except for Val6. The corresponding site in KFR of *Gluconobacter* sp. CHM43 shown in yellow complexed with NADPH (light red) was similar to that of *T. thermophilus* SDH but differed in four amino acid residues.

appears to sterically hinder the binding to the carboxyl group of shikimate. In order to examine this hypothesis, we constructed KFR derivatives having single or double amino acid replacements. Furthermore, we found that Lys72 and Asp108 in the substrate-binding site are conserved as the catalytic dyad in the SDH family (27, 28), which mediates a hydride ion transfer from the substrate to NAD(P)⁺, producing the protonated ϵ -amino group in the Lys residue. We also examined the effect of amino acid replacements in the catalytic dyad to evaluate the mechanism of KFR catalysis.

KFR belongs to a small subgroup in the shikimate dehydrogenase family. We performed a phylogenetic analysis for KFR. According to the results mentioned above, the structure of KFR is very similar to that of SDH. We retrieved homologous proteins similar to KFR, AroE-like protein of *Pseudomonas putida* (Pp_Ael1) (28, 29), aminoshikimate dehydrogenase of *P. putida* (Pp_Rif12) (30), SDH of *Thermus thermophilus* (Tt_AroE), SDH-like protein of *Haemophilus influenzae* (Hi_SdhL) (31), SDH of *Corynebacterium glutamicum* (Cg_AroE) (32), and quinate dehydrogenase of *C. glutamicum* (Cg_QDH) (33), by BLASTP on our RefSeq data set independently. All of the 1,930 protein hits were used for the phylogenetic analysis (Fig. 5). We tentatively classified the phylogenetic tree into the 12 clades, 9 of which include functionally validated proteins, while 3 clades lack functionally characterized proteins (Fig. 5 and Table S1). The clades 1, 2, 7, 8, 10, and 12 contain the members of SDH family with considerable shikimate oxidation rates (32, 34–38), whereas the clades 4 and 9 contain YdiB of *E. coli* and SdhL of *H. influenzae* with low k_{cat} values for shikimate oxidation of 0.1 and 0.2 s⁻¹, respectively (31, 34). Clade 11 contains members with moderate shikimate oxidation activity (30). KFR belongs to clade 4, which is reasonable since it oxidized shikimate slowly with a k_{cat} value of 0.028 s⁻¹. However, no quinate oxidation (at a rate lower than 0.01 s⁻¹) was observed with KFR under the conditions similar to those for the shikimate oxidation, although YdiB of *E. coli*, the representative of clade 4, oxidizes quinate at a rate of 0.05 s⁻¹ (34). As described below, KFR belongs to a subgroup within clade 4 that was termed subclade 4a and differs from other members of clade 4 (subclade 4b) in terms of conservation of the residues in the substrate-binding site (Fig. 5B).

We examined the conservation of the nine amino acid residues of the putative substrate-binding site in the homologous proteins retrieved, i.e., Asn21, Thr23, Asn66, Ser68, Lys72, Asn93, Asp108, Pro227, and Gln255 in KFR. Even though Asn21, Thr23, Ser68, and Pro227 in KFR were different from the corresponding amino acid residues in other members of the shikimate dehydrogenase family, the position of four amino acid residues, Lys72, Asn93, Asp108, and Gln255, of KFR were aligned with the corresponding residues of the other SDH family members (Fig. S4), allowing us to speculate that these nine amino acid residues form the substrate-binding site in the 1,930 retrieved homologous proteins. Clade-level analyses revealed distinct differences in the amino acid conservation patterns of several clades, including clades 4, 9, 10, 11, and 12 (Fig. S5). Since KFR differs in four of the nine amino acid residues in the substrate-binding site from those that are most frequent in the 1,930 retrieved homologous proteins (Fig. 5B), we retrieved the proteins that differ in maximally one of the nine amino acid residues found in the substrate-binding site from that of KFR. From the original 1,930 homologous proteins, we found 30 homologous proteins that show a conservation pattern in the substrate-binding site similar to that of KFR (Table S1). These 30 proteins are shown in red in the phylogenetic tree (Fig. 5A). They formed a small cluster named subclade 4a. Three of the amino acid residues, Asn21, Thr23, and Pro227, of the substrate-binding site of clade 4a differed from the corresponding positions in other clade 4 members, subclade 4b (Fig. 5B).

Ser is found in most members of the SDH family in the position corresponding to Thr23 in KFR, but Thr in this position is also found in other members of the SDH family (Fig. 5B), such as quinate dehydrogenase of *Corynebacterium glutamicum* (Cgl0424) in clade 12, which oxidizes shikimate with a k_{cat} value of 85.2 s⁻¹ (38). Therefore, we focused on two of the three residues, Asn21 and Pro227, to evaluate the impact of the amino acid substitutions on substrate binding and the kinetic properties of KFR.

Properties of the KFR derivatives. We constructed an expression system for hexahistidine-tagged KFR in *E. coli* for biochemical characterization of the KFR derivatives

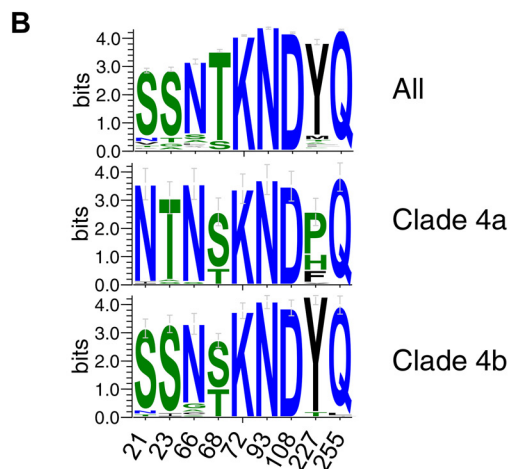
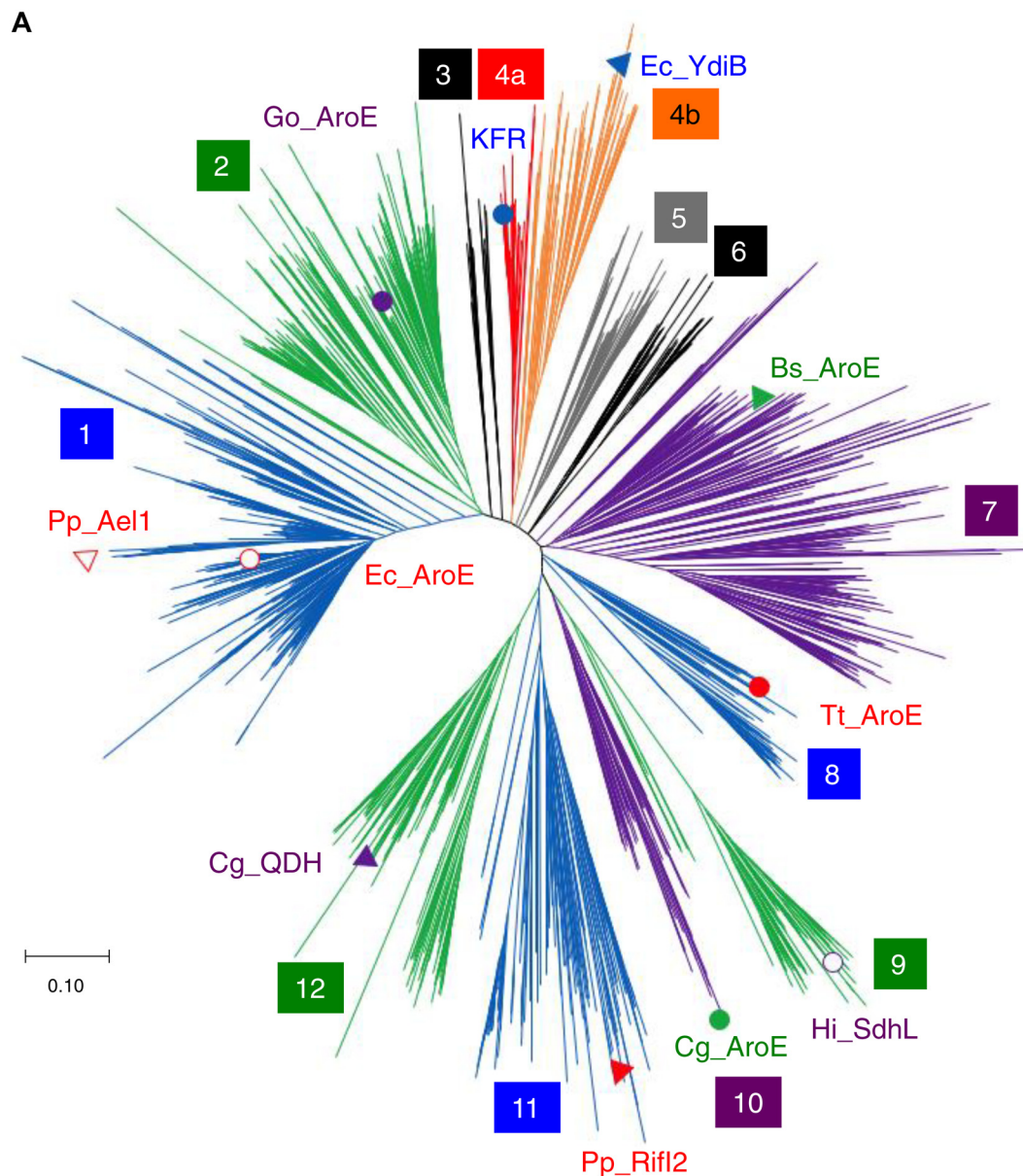


FIG 5 Phylogenetic analysis and amino acid residues in the substrate-binding site of KFR. (A) Unrooted neighbor-joining phylogenetic tree of SDH family proteins. The phylogenetic tree of 1,929 SDH homologs was constructed using the MEGAX (Continued on next page)

TABLE 2 The kinetic parameters for His-tagged KFR and its derivatives

Parameter	Sp act [U·(mg protein) ⁻¹]	V _{max} [U·(mg protein) ⁻¹]	Turnover no. (s ⁻¹) ^b	K _m (mM)	K _{cat} /K _m (s ⁻¹ mM ⁻¹) ^c
Wild type	340 ± 1	410 ± 6	680	2.1 ± 0.1	320
N21S	1.4 ± 0.1	140 ± 30	2.8	620 ± 160	0.58
P227Y	70 ± 5	220 ± 5	140	17 ± 1	28
SY	0.12 ± 0.01	NT ^a	0.25	NT	NT
K72N	0.18 ± 0.01	0.20 ± 0.005	0.36	3.4 ± 0.3	0.11
D108N	0.031 ± 0.004	0.071 ± 0.002	0.063	6.7 ± 0.7	0.0066

^aNT, not tested.

^bTurnover number was calculated from the specific activity by assuming that the KFR dimer possesses two catalytic sites from the crystal structure.

^cCatalytic efficiency (k_{cat}/K_m) was calculated from linear regression of the Lineweaver-Burk plot.

containing either single amino acid replacements of Asn21 to Ser (referred to as N21S) or Pro227 to Tyr (P227Y) and the double replacement with N21S and P227Y (SY). To evaluate the impact of the mutations on substrate binding, the kinetic properties of the KFR derivatives were determined by using 5KF as the substrate and NADPH as the cofactor. All of the KFR derivatives, including the wild-type enzyme, showed similar elution profiles in Ni²⁺-chelate affinity chromatography (Fig. S6), suggesting that the mutated KFR derivatives were expressed similarly to wild-type KFR in *E. coli*.

The N21S derivative showed a 300-fold decrease in the specific 5KF reductase activity compared to the wild-type enzyme. It also exhibited a significant change in the K_m value for 5KF, which was a 300-fold increase compared to wild-type KFR (Table 2). Similarly, the P227Y derivative showed a 5-fold decrease in the specific 5KF reductase activity. The K_m value of the P227Y derivative for 5KF was increased 8-fold. The SY derivative, which contained both the N21S and P227Y replacements, showed much lower activity than wild-type KFR, so that it was difficult to determine the kinetic parameters. As for oxidation direction, fructose dehydrogenase activities of the KFR derivatives were determined (Fig. 6). KFR catalyzes the reaction predominantly in the reduction direction using NADPH, but the K_m values of 5KF and fructose are similar to each other (Table 1) (10). The rates of fructose oxidation by the KFR derivatives were different; the P227Y derivative showed relatively high activity, but the N21S derivative showed much lower activity than wild-type KFR, and no activity was detected for the SY derivative. These amino acid replacements presumably resulted in a loss of affinity to fructose as well as loss of affinity to 5KF.

We attempted to detect 3-dehydroshikimate reductase activities in the KFR derivatives with a maximal substrate concentration of 4 mM due to the scarcity of the reagent available, but no activity was found with any of the KFR derivatives. Then, we examined NADP⁺-dependent shikimate dehydrogenase activities of the KFR derivatives (Fig. 6). There are no apparent differences in shikimate dehydrogenase activity of the P227Y and SY derivatives compared to wild-type KFR. On the other hand, the N21S derivative showed an approximately 7-fold higher shikimate dehydrogenase activity than the wild-type enzyme, whereas the fructose dehydrogenase activity was almost completely abolished by this amino acid replacement (Fig. 6). We examined the affinity

FIG 5 Legend (Continued)

v10.1.8 package (65, 66). The scale bar represents 0.1 substitution per site. The 11 experimentally validated functional sequences are designated as follows: KFR (blue circle), Ec_AroE (open red circle), Ec_YdiB (blue triangle), Pp_Ael1 (open red triangle), Pp_Rif12 (closed red triangle), Bs_AroE (green triangle), Tt_AroE (closed red circle), Hi_SdhL (open purple circle), Cg_AroE (green circle), Cg_QDH (purple triangle), and Go_AroE (filled purple circle). The tree was tentatively divided into 12 clades; clade 4 was further divided into the subclades 4a and 4b. (B) Conservations of amino acid residues in the substrate-binding sites of 1,929 proteins and in the subclades 4a and 4b were illustrated with WebLogo using stacks of symbols, one stack for each position in the sequence. The size of the symbols within the stack indicates the relative frequency of each amino acid at that position (67). KFR, GLF_2050, KFR of *Gluconobacter* sp. CHM43; Ec_AroE, b3281, SDH of *E. coli* (34); Ec_YdiB, b1692, quinate/shikimate dehydrogenase of *E. coli* (34, 70); Pp_Ael1, PP3002, AroE-like protein of *Pseudomonas putida* (28, 29); Pp_Rif12, PP_2608, aminoshikimate dehydrogenase of *Pseudomonas putida* (30); Bs_AroE, BSU25660, SDH of *Bacillus subtilis* (36); Tt_AroE, TTHA1050, SDH of *Thermus thermophilus*; Hi_SdhL, HI0607, SDH-like protein of *Haemophilus influenzae* (31); Cg_AroE, cGr_1677, SDH of *Corynebacterium glutamicum* (32); Cg_QDH, Cgl0424, quinate dehydrogenase of *C. glutamicum* (38); Go_AroE, GOX_1959, SDH of *Gluconobacter oxydans* (35).

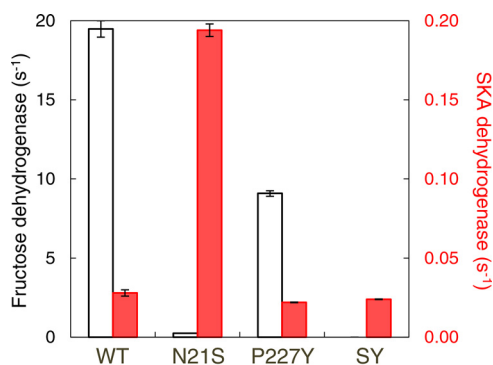


FIG 6 Replacement Asn21 to Ser in KFR improves shikimate dehydrogenase activity. Fructose (white bars) and shikimate (red bars) dehydrogenase activities of the KFR derivatives were examined in the presence of NADP⁺. Turnover number was calculated from the specific activity by assuming that the KFR dimer possesses two catalytic sites from the crystal structure.

to shikimate of the N21S derivative, but it seemed similar to that of wild-type KFR. Therefore, we considered that the elevated catalytic efficiency of the N21S derivative was derived from the elevated specific activity to shikimate (Fig. S7).

In order to explore the catalytic mechanism of KFR, either the Lys72 or Asp108 residue was replaced with Asn. The replacement of Lys and Asp with Asn may minimize the changes in side chain van der Waals volumes but can eliminate the functions of Lys and Asp in general acid-base catalysis (27, 28). We determined the kinetic parameters of the KFR derivatives with 5KF as the substrate and NADPH as cofactor (Table 2). The K72N and D108N derivatives exhibited approximately 1,900- and 11,000-fold decreased turnover numbers compared to the wild-type enzyme. Nonetheless, both KFR variants showed only minor changes in the K_m values for 5KF, which were only 1.6- and 3.2-fold increases compared to the wild-type enzyme (Table 2). Therefore, these results support a role of the Lys72 and Asp108 residues in the catalytic mechanism of KFR.

DISCUSSION

SDH is one of the crucial enzymes in the shikimate pathway in plants and microbes, which is required for the biosynthesis of aromatic amino acids and other aromatic compounds. The SDH family is a large protein family containing at least five discrete enzymes, AroE as typical SDH, YdiB (QDH), aminoshikimate dehydrogenase RflI, SDH-like protein SdhL, and AroE-like1 Ael1 (39). We examined the structure, phylogeny, and enzymatic properties of KFR in this study. Although it has unique properties in the substrate specificity, the overall structure of the KFR protein and the amino acid residues responsible for NADPH binding were highly similar to those of members of the SDH family. We also identified the unique amino acid residues that are important for 5KF recognition. Considering these data together, we suggest that KFR of *Gluconobacter* spp. is a member of a subclass in the SDH family.

We revealed that the *GLF_2050* gene encodes KFR, which is responsible for most of the cellular KFR activity and is physiologically relevant to 5KF metabolism *in vivo*. KFR would reduce 5KF with NADPH to fructose and supply it to the pentose phosphate pathway when *Gluconobacter* sp. CHM43 grows on mannitol. The Δkfr (ΔGLF_2050) strain still possessed approximately 29% of the KFR activity of the wild-type CHM43 strain, suggesting that the Δkfr strain has at least one gene responsible for the remaining KFR activity. Despite the residual KFR activity, the Δkfr strain did not consume 5KF in our cultivation conditions, while the wild-type strain and the complemented Δkfr mutant consumed it (Fig. 2). These results suggest that the *GLF_2050* gene encodes the KFR protein that is relevant to 5KF metabolism *in vivo*.

We attempted to propose a possible route for the development of KFR in evolution. The overall structure of KFR was similar to that of SDH (Fig. 3). Although we failed to

obtain a structure for a 5KF-bound form of KFR, we deduced the nine amino acid residues for substrate binding based on the structural similarity to a substrate-bound form of SDH (37, 40). Of the nine amino acid residues involved in substrate binding by SDH, four were different in KFR, which is consistent with the different substrate specificities of the two enzymes. When we examined the conservation of nine amino acid residues proposed to be involved in substrate binding by KFR in the members of the SDH family (see Fig. S4 and S5 in the supplemental material), the homologs having similar patterns to KFR clustered in the clade 4a. In clade 4b, which includes *E. coli* quinate/shikimate dehydrogenase YdiB, three of the nine residues differ from those in clade 4a (Fig. 5). Thus, we suggest that KFR is derived from a primordial protein of clade 4, which evolved to enable accommodation of 5KF. The HA49_09215 protein of *Tatumella morbirosei*, one of the KFRs that Schiessl et al. characterized, belongs to the SDH family (19). The HA49_09215 protein and *Tatumella citrea* KFR (A7K98_06190) characterized previously (41) and the DW_RS0115250 protein of *Tatumella saanichensis* that is found in our list of the SDH family (Table S1) and belongs to clade 4a in the phylogenetic analysis of Fig. 5 are highly homologous with greater than 90% similarity to one another. The nine amino acid residues involved in substrate binding in the three *Tatumella* KFRs are identical to those of GLF_2050 (Fig. S8).

Based on the assumption mentioned above, we attempted to enhance reactivity of KFR to shikimate or dehydroshikimate by site-directed mutagenesis at the substrate-binding site. Wild-type KFR can oxidize shikimate only at an extremely low rate (Fig. 6), while partially purified SDH of *G. oxydans* (Go_AroE: GOX1959) with shikimate oxidation activity of $24 \text{ U} \cdot (\text{mg protein})^{-1}$ showed no 5KF reduction activity [at a rate lower than $0.0018 \text{ U} \cdot (\text{mg protein})^{-1}$]. Analysis of the P227Y derivative of KFR revealed the importance of Pro227 for 5KF binding by a 5-fold decreased turnover number and an 8-fold increased K_m value for 5KF (Table 2). However, the P227Y substitution resulted in SDH activity similar to that of wild-type KFR (Fig. 6). The N21S derivative showed a 300-fold increase in the K_m value for 5KF, suggesting a crucial function of Asn21 in 5KF recognition (Table 2). Because the N21S derivative showed a 7-fold increase in the shikimate oxidation activity, the N21S substitution somehow enhances the catalytic efficiency of shikimate oxidation. More detailed biochemical and structural analyses are needed to understand how this amino acid substitution increases the reaction rate.

To understand the catalytic mechanism of 5KF reduction, we examined catalytic efficiency of the KFR derivatives that have the amino acid replacements in the catalytic dyad Lys72 and Asp108 with Asn (27, 28, 40). Both amino acid replacements resulted in large decreases in the V_{\max} value but small impacts on the K_m value for 5KF, suggesting that they affect the rate of catalysis but not substrate binding. From these results, we suggest the catalytic mechanism of 5KF reduction by KFR, under which Lys72 is protonated by the action of Asp108 to protonate C5 carbonyl oxygen of 5KF. NADPH transfers hydride ion to the protonated 5KF to yield fructose and NADP^+ , as suggested in SDHs of *T. thermophilus* and *Aquifex aeolicus* (37, 40).

The structure of the substrate for KFR is a subject of debate. It was reported that gem-diol hydrate is the major form of 5KF in solution, which had been isolated from *Gluconobacter* cultures (42, 43). However, the reduction of the gem-diol hydrate form is chemically impossible in the reaction catalyzed by KFR. Blanchard et al. (42) detected a chain form of 5KF in solution at 70°C , suggesting that this as a minor form of 5KF. It is plausibly considered that 5-keto-D-fructopyranose is a possible intermediate in equilibrium between the gem-diol hydrate and the chain form (Fig. S9). We constructed modeled structures of the substrate-bound KFR with the three possible forms of 5KF, i.e., the pyranose, chain, and gem-diol hydrate forms (Fig. S10). The pyranose and chain forms of 5KF seem to be accommodated in the substrate-binding site in KFR. However, Leu252 would be close to the hydroxyl group specific in the gem-diol hydrate form within 3.0 \AA , which may sterically hinder the binding itself. Thus, the structure modeling for the substrate-bound KFR supports that the substrate for KFR is the pyranose and chain forms, even if the gem-diol hydrate is the predominant form of 5KF in

TABLE 3 *Gluconobacter* strains and plasmids used in this study

Strains and plasmids	Relevant characteristics	Source or reference
<i>Gluconobacter</i> strains		
ATCC 621H	<i>Gluconobacter oxydans</i> wild type	ATCC
CHM43	Wild type	2
NMT912	CHM43 Δkfr	This study
Plasmids		
pKOS6b	Suicide vector, <i>mob codAB</i> Km ^r	52
pCM62	Broad-host-range vector, <i>mob</i> Tc ^r	51
pTTQ18	Expression vector, <i>lacI</i> ^Q P _{lac} Ap ^r	71
pJY19	pTTQ18, opposite orientation of multiple cloning site	49
pBBR1MCS-4	Broad-host-range vector, <i>mob</i> Ap ^r	50
pSHO8	pBBR1MCS-4, promoter for the <i>adhAB</i> gene of <i>G. oxydans</i> ATCC 621H	5
pET3a	Expression vector, P _{T7} Ap ^r	Novagen
pNMT91	pKOS6b Δkfr	This study
pNMT72	pSHO8 <i>kfr</i> (<i>GLF_2050</i>)	This study
pNMT4	pJY19 <i>kfr</i> (<i>GLF_2050</i>)	This study
p9KX6264	pCM62, promoter for the <i>adhAB</i> gene of <i>G. oxydans</i> ATCC 621H, <i>kfr</i> (<i>GLF_2050</i>)	This study
pbqNK1	pTTQ18 <i>his-kfr</i>	This study
pJ808	pET3a, <i>aroE</i> ^a (<i>GOX1959</i>) of <i>G. oxydans</i> ATCC 621H	This study

^a*aroE*, the gene for shikimate dehydrogenase.

solution. Because dihydroxyacetone was reduced by KFR (see Results), the chain form of 5KF might be favored as the substrate for KFR.

MATERIALS AND METHODS

Chemicals. 5-Keto-fructose (5KF) was supplied by Kyowa-Hakko Bio (Tokyo, Japan). 5-Fluorocytosine was purchased from Fluorochem (Glossop, UK). 3-Dehydroshikimate was prepared from quininate as described previously (44). All other materials used were of analytical grade and obtained from commercial sources.

Bacterial strains and culture conditions. *Escherichia coli* strain DH5 α was used for plasmid construction (45). The BL21 and BL21(DE3)/pLys strains were used for protein expression (46, 47). The *Gluconobacter* strains and plasmids used in this study are listed in Table 3. *Gluconobacter* sp. strain CHM43 and its derivatives were cultivated routinely at 30°C with shaking (200 rpm) in Δ P medium consisting of 5 g of D-glucose, 20 g of glycerol, 10 g of yeast extract (Oriental Yeast, Tokyo, Japan), and 10 g of hipolypepton (Nihon Pharmaceuticals, Osaka, Japan) per liter; mannitol medium consisting of 50 g of D-mannitol, 3 g of yeast extract, and 3 g of hipolypepton per liter; or fructose medium consisting of 40 g of D-fructose, 3 g of yeast extract, and 3 g of hipolypepton per liter. For the strain construction, the CHM43 strain was cultivated on sorbitol medium consisting of 50 g of D-sorbitol, 3 g of yeast extract, and 3 g of hipolypepton per liter. *Escherichia coli* strains were cultivated in Luria-Bertani (LB) medium at 30°C. Ampicillin was used at final concentrations of 50 and 500 μ g ml⁻¹ for *E. coli* and *Gluconobacter*, respectively. Kanamycin and tetracycline were used at final concentrations of 50 μ g ml⁻¹ and 10 μ g ml⁻¹, respectively.

Construction of plasmids. The genomic DNA of *Gluconobacter* sp. strain CHM43 was isolated by the method of Marmur (48) with some modifications (5). The *GLF_2050* gene was amplified by PCR with the Herculase II fusion DNA polymerase (Stratagene, CA, USA), the CHM43 genomic DNA, and a pair of oligonucleotides, ex-*GLF_2050*-5-Hin(+) and ex-*GLF_2050*-3-Xba(-) (Table 4). The PCR product was inserted into the HindIII and XbaI sites of pJY19 (49) and pSHO8 (5), a derivative of the broad-host-range vector pBBR1MCS-4 (50), carrying a promoter region for the *adhAB* gene of *G. oxydans* ATCC 621H, to construct pNMT4 and pNMT72, respectively. The 1.7-kb KpnI and XbaI fragment of pNMT72 that carries the *adhAB* promoter and the *GLF_2050* gene was inserted in the corresponding sites of pCM62 (51) to construct p9KX6264.

To delete the *GLF_2050* gene in the CHM43 strain, the homologous arms in the 5' and 3' regions of the *GLF_2050* gene were amplified using two sets of oligonucleotides, Δ GLF_2050-5-Kpn(+) and Δ GLF_2050-5-RI(-) for the 5' region and Δ GLF_2050-3-RI(+) and Δ GLF_2050-3-Xba(-) for the 3' region. The two PCR products were inserted into the KpnI and XbaI sites of the suicide vector pKOS6b (52) to construct pNMT91.

The N-terminally hexahistidine-tagged *GLF_2050* was constructed by PCR with the oligonucleotide RI-His6-3C-kfr(+). The PCR product was inserted into the HindIII and XbaI sites of pTTQ18 to construct pbqNK1. The amino acid replacements in the *GLF_2050* gene were constructed by PCR with the pairs of oligonucleotides listed in Table 4, followed by DpnI treatment.

The *GOX1959* gene was amplified by PCR using the genome DNA of *Gluconobacter oxydans* ATCC 621H and a pair of oligonucleotides, *GOX1959*-5-Eco(+) and *GOX1959*-3-SphBgl(-). The PCR product was inserted into the NdeI and BamHI sites of pET3a (Novagen, Darmstadt, Germany) to construct

TABLE 4 Oligonucleotides used in this study

Name	Sequence (5' → 3') ^a	Objective ^b
ex-GLF_2050-5-Hin(+)	<u>aagctt</u> cagagacagtctcgaataag	<i>kfr</i> ⁺
ex-GLF_2050-3-Xba(-)	tctagatggtatgaaaaccctgc	<i>kfr</i> ⁺
ΔGLF_2050-5-Kpn(+)	<u>ggtacc</u> cattacgcgactgaag	Δ <i>kfr</i>
ΔGLF_2050-5-Rl(-)	<u>gaattc</u> caccatcgccacggtag	Δ <i>kfr</i>
ΔGLF_2050-3-Rl(+)	<u>gaattc</u> ggaacagaaaataagtaagc	Δ <i>kfr</i>
ΔGLF_2050-3-Xba(-)	tctagaaggcagaattacttctcg	Δ <i>kfr</i>
Rl-His6-3C-kfr(+)	<u>gaattc</u> gcatcaccatcaccatcacctggaagtctgttcaggggcccagcggacaaggctt	N-His6
5KFR-N21S(+)	caccctcgccgacTcctaccgtggcgatg	N21S
5KFR-N21S(-)	catcgccacggtaggaGAgtcgcgccagggggtg	N21S
5KFR-P227Y(+)	gttgcggtgctattTAcacccgcctcagac	P227Y
5KFR-P227Y(-)	gtctgaggcgggttgTAaatgacatccgcaac	P227Y
5KFR-K72N(+)	ctccctgcccacaaCgtcgccgttctcgatc	K72N
5KFR-K72N(-)	gatcgagaacggcgacGttgtggggcagggag	K72N
5KFR-D108N(+)	gattggtcataaactAaTggcaagggtcttc	D108N
5KFR-D108N(-)	gaaagcccttgccAtTagtgttatgaccaatc	D108N
GOX1959-5-Eco(+)	<u>gaattc</u> catatgattgacggtcacacgaaac	<i>aroE</i>
GOX1959-3-SphBgl(-)	<u>agatct</u> gcatcgccgaccgtacttttc	<i>aroE</i>

^aRecognition sites for the restriction endonucleases (KpnI, EcoRI, XbaI, HindIII, NdeI, SphI, and BglII) are underlined. Uppercase letters show substituted bases.

^bΔ*kfr*, construction of the Δ*kfr* strain; *kfr*⁺, construction of the expression plasmid; N-His6, construction of the gene for N-terminally hexahistidine-tagged KFR.

pJ808. Nucleotide sequences of all DNA fragments inserted into the plasmids were confirmed by the Sanger method (BigDye Terminator v3.1 cycle sequencing kit; Applied Biosystems, Foster City, CA, USA).

Transformation of *Gluconobacter* sp. strain CHM43 and the construction of the gene deletion variant. The CHM43 strain was transformed with the plasmids constructed in this study via electroporation and selected on sorbitol agar medium with the appropriate antibiotics as described previously (53). In the case of the construction of the *kfr* gene deletion variant, the recombinant strain obtained after the first homologous recombination was inoculated on sorbitol agar medium containing 60 μg ml⁻¹ 5-fluorocytosine to select the strains with a second homologous recombination event as described previously (52, 53).

Determination of fructose, 5KF, and acetic acid in the culture medium. The bacterial culture was taken and centrifuged at 10,000 × *g* for 5 min at 4°C to remove the cells. The supernatant was filtered with a filter with 0.4-μm-size pores (Merck Millipore, Burlington, MA, USA). The filtered supernatant was analyzed using a high-performance liquid chromatography (HPLC) system equipped with a refraction index (RI) detector and a photodiode array (PDA). Fructose, 5KF, and acetic acid were separated on an ion-exclusion column (RSpak KC-811, 8.0 mm inside diameter by 300 mm length; Shodex, Showa Denko KK, Kawasaki, Japan) at 60°C using 0.1% (wt/vol) phosphoric acid as a mobile phase at a flow rate 0.4 ml min⁻¹. Fructose and acetic acid were detected by RI, while 5KF was detected by PDA at 210 nm. The retention times on fructose, 5KF, and acetic acid were 19.9, 18.1, and 26.9 min, respectively. Fructose and 5KF were determined by the calibration curves based on the peak heights of the compounds on the chromatograms, while acetic acid was determined by the peak squares.

We determined evaporation factors to accurately estimate the optical density at 600 nm (OD₆₀₀) value and the amounts of fructose, 5KF, and acetic acid by measuring fructose levels in abiotic incubation of the fructose medium as follows: 0 h, 1.00 ± 0.009; 0.5 days, 1.02 ± 0.009; 1 day, 1.02 ± 0.01; 2 days, 1.04 ± 0.007; 3 days, 1.05 ± 0.008; 4 days, 1.06 ± 0.007; 5 days, 1.07 ± 0.008; 6 days, 1.08 ± 0.01; 7 days, 1.10 ± 0.01; 8 days, 1.13 ± 0.012; 9 days, 1.14 ± 0.008; 10 days, 1.15 ± 0.01. We modified the OD₆₀₀ value and the concentrations of fructose, 5KF, and acetic acid in the culture medium with the evaporation factors.

Purification of native KFR. *Gluconobacter* sp. strain CHM43 harboring pNMT72 was cultured in 500 ml mannitol medium containing 500 μg ml⁻¹ ampicillin with shaking at 30°C until the late exponential phase of growth. Cells were harvested by centrifugation at 10,000 × *g* for 10 min at 4°C, followed by washing with 10 mM K⁺-phosphate (pH 6.0) containing 1 mM β-mercaptoethanol (β-ME). The cells were suspended in the same buffer and passed through a French pressure cell press (1,100 kg cm⁻²) twice. Intact cells and cell debris were removed by centrifugation at 10,000 × *g* for 10 min at 4°C, and the membranes were removed from the supernatant by ultracentrifugation at 100,000 × *g* for 1 h at 4°C. The soluble fraction was applied to a DEAE-cellulose column equilibrated with 10 mM K⁺-phosphate (pH 6.0) containing 1 mM β-ME. After the column was washed with the same buffer, KFR was eluted using a linear gradient system that consisted of 10 and 200 mM K⁺-phosphate (pH 6.0) containing 1 mM β-ME. The collected active fractions were dialyzed with 10 mM K⁺-phosphate (pH 6.0) containing 1 mM β-ME. The dialysate was applied to a ceramic hydroxyapatite (Bio-Rad) column, which had been equilibrated with the same buffer. The enzyme was eluted with a linear gradient system consisting of 100 and 300 mM K⁺-phosphate (pH 6.0) containing 1 mM β-ME. In order to concentrate the protein, the collected active fractions were dialyzed and applied to a small DEAE-cellulose column and eluted by 200 mM K⁺-phosphate (pH 6.0) containing 1 mM β-ME. The fraction with the highest activity was dialyzed to 10 mM K⁺-phosphate (pH 6.0) containing 1 mM β-ME and was used for crystallization and other enzyme characterization.

TABLE 5 Data collection and processing^a

Crystal	Ligand free	NADPH complex
Diffraction source	KEK, PF, BL1A	KEK, PF-AR, NW12A
Wavelength (Å)	1.1000	1.0000
Temp (K)	100	95.0
Detector	Eiger X4M	ADSC Quantum270r
Crystal-detector distance (mm)	74.63	244.00
Rotation range per image (°)	0.5	0.5
Total rotation range (°)	240	150
Exposure time per image (s)	1.0	2.0
Space group	<i>P</i> 2 ₁	<i>P</i> 2 ₁
<i>a</i> , <i>b</i> , <i>c</i> (Å)	41.53, 63.47, 93.92	40.50, 61.53, 96.86
α , β , γ (°)	90.00, 93.42, 90.00	90.00, 96.82, 90.00
Mosaicity (°)	0.20	0.60
Resolution range (Å)	41.45–1.50 (1.58–1.50)	40.21–1.95 (2.06–1.95)
Total no. of reflections	351,914	105,580
No. of unique reflections	77,600	33,451
Completeness (%)	99.5 (99.8)	96.7 (93.1)
<i>R</i> _{merge}	0.094 (0.510)	0.060 (0.151)
Redundancy	4.5 (4.7)	3.2 (3.0)
$\langle I/\sigma(I) \rangle$	9.4 (3.6)	13.1 (6.3)
<i>R</i> _{r.i.m.}	0.107 (0.577)	0.072 (0.184)
Overall B factor from Wilson plot (Å ²)	13.941	20.890

^aValues for the outer shell are given in parentheses.

Gel filtration column chromatography. The purified enzyme was loaded on a Superdex 200 column that had been equilibrated with 10 mM K⁺-phosphate (pH 6.0) containing 0.1 M NaCl and 1 mM β -ME. The native molecular mass of KFR was determined by a calibration curve of a standard marker protein mixture (Oriental Yeast, Tokyo, Japan), which comprised yeast glutamate dehydrogenase (290 kDa), pig heart lactate dehydrogenase (142 kDa), yeast enolase (67 kDa), yeast myokinase (32 kDa), and horse heart cytochrome *c* (12.4 kDa).

Crystallization, data collection, and structural determination of KFR. For crystallization, purified KFR from the recombinant *Gluconobacter* sp. strain CHM43 was used. Initial sparse matrix crystallization screening was performed at 295 K, by hanging-drop vapor diffusion, with 4- μ l drops of enzyme against reservoir solution, using a Hampton PEG/Ion screen kit. Native (ligand-free) KFR was crystallized using 7.6 mg/ml enzyme solution and 18% (wt/vol) PEG3350, 0.95 M HEPES-Na (pH 8.0), 140 mM calcium acetate, 4.5% (vol/vol) ethylene glycol, and 5% (vol/vol) 1,4-butanediol as the reservoir solution. For crystallization of the KFR-NADPH complex, drops were prepared by mixing 2 μ l of enzyme solution (17 mg/ml) with 1 μ l of 20 mM NADPH and 2 μ l of reservoir solution and were equilibrated against 100 μ l of reservoir solution at room temperature. Crystals were obtained in 16% (wt/vol) PEG3350, 45 mM HEPES-Na (pH 7.5), 180 mM ammonium fluoride, and 19% (vol/vol) 2-methyl-2,4-pentanediol (MPD). The crystals under both conditions appeared after 1 week and grew to the size used for the measurement in 2 weeks. The crystal size used for the X-ray diffraction were approximately 0.13 by 0.07 by 0.02 mm³.

The X-ray diffraction data sets for the native KFR crystal and KFR-NADPH complex crystal were collected from the Synchrotron Radiation Source at the PF beam line BL1A and the PF-AR beam line NW12A (Tsukuba, Japan). Prior to measurement, the KFR crystals were dipped in a cryoprotectant with 15% glycerol and flash-cooled in a stream of cool nitrogen gas at 95 to ~100 K. As for the KFR-NADPH complex, since the reservoir contained MPD, the crystals were used without additional cryoprotectant. The native KFR crystal diffracted to 1.50 Å in cell dimensions of *a* = 41.53 Å, *b* = 63.47 Å, *c* = 93.92 Å, and β = 93.42° with the space group of *P* 2₁. The KFR-NADPH complex crystal diffracted to 1.95 Å in cell dimensions of *a* = 40.50 Å, *b* = 61.53 Å, *c* = 96.86 Å, and β = 96.82° with the space group of *P* 2₁. Processing and scaling were performed with the program XDS (54) scaling with POINTLESS (55, 56) and SCALA (55) of CCP4 (23). The parameters of data collection and processing are summarized in Table 5. The structure was solved by molecular replacement using MOLREP (57) with an initial model of SDH from *Methanocaldococcus jannaschii* (PDB entry 1NVT [58]). The structure was manually built in COOT (24) and refined with REFMAC5 (59) with subsequent rounds of model building, refinement, and structural analysis until *R*_{work} and *R*_{free} of native KFR stabilized to 0.23 and 0.25, respectively. The structure of the KFR-NADPH complex was refined until *R*_{work} and *R*_{free} stabilized to 0.21 and 0.26, respectively (Table 6). Electron density for NADPH could be clearly seen in the NADPH-binding pocket. The final structural coordinates and electron density maps were deposited in the Protein Data Bank (PDB codes 7COK and 7COL for the ligand-free and NADPH complex forms, respectively). Structural visualization was performed in CCP4mg (60).

We constructed modeled structures of the substrate-bound KFR-NADPH complex on COOT using *Thermus* SDH-NADP(H)-shikimate complex (2EV9) (37). Each 5KF form was manually placed on the substrate-binding site of the KFR-NADPH complex by comparing 5KF and shikimate on the *Thermus* SDH, particularly three hydroxyl groups on C3, C4, and C5 of 5KF and C3, C4, and C5 of shikimate. The structural coordinates of the substrate were prepared using PRODRG (61).

TABLE 6 Structure solution and refinement^a

Crystal	Ligand free	NADPH complex
Resolution range (Å)	41.453–1.500	40.213–1.950
Completeness (%)	99.367	96.440
σ cutoff	0	0
No. of reflections, working set	73,708	31,710
No. of reflections, test set	3,862	1,723
Final R_{work}	0.2319	0.2085
Final R_{free}^b	0.2544	0.2637
No. of non-H atoms		
Protein	3,992	4,005
Ligand (NADPH)		96
Water	231	399
RMS deviations ^c		
Bonds (Å)	0.0092	0.0092
Angles (°)	1.3870	1.4284
Avg B factors (Å ²)		
Protein	17.66	23.40
Ligand (NADPH)		33.97
Water	24.45	33.31
Ramachandran plot		
Most favored (%)	98.9	97.8
Allowed (%)	1.1	2.0

^aValues for the outer shell are given in parentheses.

^b R_{free} was monitored with 5% of the reflection data excluded from the refinement.

^cRMS, root mean square.

Purification of the KFR derivatives. The N-terminally hexahistidine-tagged KFR and the derivatives with amino acid replacements were expressed in *E. coli* BL21 grown in 100 ml of LB medium containing 50 $\mu\text{g ml}^{-1}$ ampicillin. The recombinant *E. coli* cells were cultivated at 30°C for 12 h, and then isopropyl- β -D-thiogalactopyranoside (IPTG) was added to the final concentration of 1 mM to induce the synthesis of His-tagged KFR by additional cultivation at 30°C for 12 h. Cells were collected by centrifugation at 10,000 $\times g$ for 10 min at 4°C and washed twice with 20 mM Na⁺-phosphate (pH 7.8) containing 500 mM NaCl. Cells were disrupted with a French pressure cell press, and then the soluble fraction was obtained by ultracentrifugation as described above. The soluble fraction (1 ml) was mixed with 40 μl of nickel-nitrilotriacetic (Ni-NTA) affinity beads (Toyobo, Tokyo, Japan). The beads were washed twice with 20 mM Na⁺-phosphate (pH 6.0) containing 500 mM NaCl and 10 mM imidazole. The His-tagged KFR was eluted with 20 mM Na⁺-phosphate (pH 6.0) containing 500 mM NaCl and 75 mM imidazole.

Enzyme assay and kinetics. KFR activity was measured by monitoring the oxidation of 0.1 mM NADPH at 340 nm with 5 mM 5KF in 50 mM K⁺-phosphate (pH 7.5) in a total reaction volume of 1 ml at 25°C. The oxidation reactions were measured by monitoring the reduction of 0.25 mM NADP⁺ at 340 nm with 10 mM fructose or 100 mM shikimate in 50 mM Na⁺-glycine buffer (pH 10) in a total reaction volume of 1 ml at 25°C. The background activity without substrate (5KF, fructose, and shikimate) was monitored, which was subtracted from the activity with substrate to calculate the net activity. The V_{max} and K_m values were determined on KaleidaGraph v4.5 (Synergy Software, Reading, PA, USA).

Sequence data retrieval and phylogenetic tree construction. The 1,964 genome sequences (one genus per one genome) were downloaded from the NCBI Reference Sequence (RefSeq) FTP website at <ftp.ncbi.nlm.nih.gov/genomes/refseq/>. For phylogenetic analysis, we performed a BLASTP search against all protein-coding sequences from the 1,964 genomes using amino acid sequences of 6 functionally validated protein sequences, GLF_2050, AroE-like protein of *Pseudomonas putida* (Pp_Ae1) (28, 29), amino-shikimate dehydrogenase of *Pseudomonas putida* (Pp_Rif2) (30), SDH of *Thermus thermophilus* (Tt_AroE), SDH-like protein of *Haemophilus influenzae* (Hi_SdhL) (31), SDH of *Corynebacterium glutamicum* (Cg_AroE) (32), and quininate dehydrogenase of *C. glutamicum* (Cg_QDH) (33) as the query (62). The homologous set was selected with a BLASTP filtering expectation value (E value) of $\leq 10^{-10}$ and sequence overlap of $\geq 70\%$. All homologous hits from each query were collected, and the merged unique sequence data set was used for phylogenetic tree construction. Input amino acid sequences were aligned using MUSCLE v3.8.31 and used for phylogenetic construction (63, 64). The MEGAX v10.1.8 package was used to generate the phylogenetic tree to study the phylogenetic relationships using the neighbor-joining (NJ) approach (65, 66). Functionally validated protein sequences used as the queries for the BLASTP searches were also included in the phylogenetic analysis.

Visualization of consensus sequences in active sites from each phylogenetic clade. The nine active site amino acid residues from each phylogenetic clade were used as input into WebLogo to assess the common consensus sequence. The sequences were illustrated with WebLogo using stacks of

symbols, one stack for each position in the sequence. The size of the symbols within the stack indicates the relative frequency of each amino acid at that position (67).

SUPPLEMENTAL MATERIAL

Supplemental material is available online only.

SUPPLEMENTAL FILE 1, PDF file, 7.5 MB.

SUPPLEMENTAL FILE 2, XLSX file, 1.1 MB.

ACKNOWLEDGMENTS

We thank Kyowa-Hakko Bio (Tokyo, Japan) and Oriental Yeast (Tokyo, Japan) for kind gifts of 5KF and yeast extract, respectively. We thank Akira Koshigashi (Toho University) for his technical assistance. We thank Mamoru Yamada and Tomoyuki Kosaka (Yamaguchi University) for their invaluable suggestions. We thank Michael Bott (Forschungszentrum Jülich) for reading and correcting the manuscript thoroughly.

We are grateful for Japanese government (Monbukagakusho: MEXT) scholarships supporting T.M.N.'s work on this study. This work was partially supported by the Japan Society for the Promotion of Science KAKENHI Grant (26450095 to T.Y.). Part of this work was performed through collaboration within the Core to Core Program, which was supported by the Japan Society for the Promotion of Science (JSPS) and Can Tho University, Vietnam.

REFERENCES

- Richhardt J, Bringer S, Bott M. 2012. Mutational analysis of the pentose phosphate and Entner-Doudoroff pathways in *Gluconobacter oxydans* reveals improved growth of a $\Delta edd \Delta eda$ mutant on mannitol. *Appl Environ Microbiol* 78:6975–6986. <https://doi.org/10.1128/AEM.01166-12>.
- Moonmangmee D, Adachi O, Ano Y, Shinagawa E, Toyama H, Theeragool G, Lotong N, Matsushita K. 2000. Isolation and characterization of thermo-tolerant *Gluconobacter* strains catalyzing oxidative fermentation at higher temperatures. *Biosci Biotechnol Biochem* 64:2306–2315. <https://doi.org/10.1271/bbb.64.2306>.
- Matsushita K, Fujii Y, Ano Y, Toyama H, Shinjoh M, Tomiyama N, Miyazaki T, Sugisawa T, Hoshino T, Adachi O. 2003. 5-keto-D-gluconate production is catalyzed by a quinoprotein glycerol dehydrogenase, major polyol dehydrogenase, in *Gluconobacter* species. *Appl Environ Microbiol* 69:1959–1966. <https://doi.org/10.1128/AEM.69.4.1959-1966.2003>.
- Ameyama M, Shinagawa E, Matsushita K, Adachi O. 1981. D-Fructose dehydrogenase of *Gluconobacter industrius*: purification, characterization, and application to enzymatic microdetermination of D-fructose. *J Bacteriol* 145:814–823. <https://doi.org/10.1128/jb.145.2.814-823.1981>.
- Kawai S, Goda-Tsutsumi M, Yakushi T, Kano K, Matsushita K. 2013. Heterologous overexpression and characterization of a flavoprotein-cytochrome c complex fructose dehydrogenase of *Gluconobacter japonicus* NBRC3260. *Appl Environ Microbiol* 79:1654–1660. <https://doi.org/10.1128/AEM.03152-12>.
- Richhardt J, Luchterhand B, Bringer S, Büchs J, Bott M. 2013. Evidence for a key role of cytochrome bo_3 oxidase in respiratory energy metabolism of *Gluconobacter oxydans*. *J Bacteriol* 195:4210–4220. <https://doi.org/10.1128/JB.00470-13>.
- Matsushita K, Toyama H, Adachi O. 1994. Respiratory chains and bioenergetics of acetic acid bacteria. *Adv Microb Physiol* 36:247–301. [https://doi.org/10.1016/s0065-2911\(08\)60181-2](https://doi.org/10.1016/s0065-2911(08)60181-2).
- Adachi O, Nguyen TM, Hours RA, Kataoka N, Matsushita K, Akakabe Y, Yakushi T. 2020. 5-Keto-D-fructose production from sugar alcohol by isolated wild strain *Gluconobacter frateurii* CHM 43. *Biosci Biotechnol Biochem* 84:1745–1747. <https://doi.org/10.1080/09168451.2020.1767500>.
- Aida K, Yamada Y. 1964. A new enzyme, 5-ketofructose reductase. *Agric Biol Chem* 28:74–75. <https://doi.org/10.1080/00021369.1964.10858208>.
- Avigad G, Englard S, Pifko S. 1966. 5-Keto-D-fructose. IV. A specific reduced nicotinamide adenine dinucleotide phosphate-linked reductase from *Gluconobacter cerinus*. *J Biol Chem* 241:373–378. [https://doi.org/10.1016/S0021-9258\(18\)96926-7](https://doi.org/10.1016/S0021-9258(18)96926-7).
- Ameyama M, Matsushita K, Shinagawa E, Adachi O. 1981. 5-Keto-D-fructose reductase of *Gluconobacter industrius*: purification, crystallization and properties. *Agric Biol Chem* 45:863–869. <https://doi.org/10.1271/bbb1961.45.863>.
- Prust C, Hoffmeister M, Liesegang H, Wiezer A, Fricke WF, Ehrenreich A, Gottschalk G, Deppenmeier U. 2005. Complete genome sequence of the acetic acid bacterium *Gluconobacter oxydans*. *Nat Biotechnol* 23:195–200. <https://doi.org/10.1038/nbt1062>.
- Terada O, Suzuki S, Kinoshita S. 1961. Formation of 5-dehydrofructose by members of *Acetobacter*. Part III. Characterization of the unknown substance. *J Agric Chem Soc Jpn* 35:178–182. <https://doi.org/10.1271/nogeikagaku1924.35.3.178>.
- Wyrobnik DH, Wyrobnik IH, Silcoff ER. 5 March 2009, filing date. Agent for reducing the useable calorie content of food and for therapeutic reduction of weight, in particular for use in the case of adiposity (obesity). US patent application 20,090,060,956.
- Barbe JC, De Revel G, Joyeux A, Bertrand A, Lonvaud-Funel A. 2001. Role of botrytized grape micro-organisms in SO₂ binding phenomena. *J Appl Microbiol* 90:34–42. <https://doi.org/10.1046/j.1365-2672.2001.01200.x>.
- Adachi O, Ano Y, Shinagawa E, Matsushita K. 2008. Purification and properties of two different dihydroxyacetone reductases in *Gluconobacter suboxydans* grown on glycerol. *Biosci Biotechnol Biochem* 72:2124–2132. <https://doi.org/10.1271/bbb.80199>.
- Matsumoto N, Hattori H, Matsutani M, Matayoshi C, Toyama H, Kataoka N, Yakushi T, Matsushita K. 2018. A single-nucleotide insertion in a drug transporter gene induces a thermotolerance phenotype in *Gluconobacter frateurii* by increasing the NADPH/NADP⁺ ratio via metabolic change. *Appl Environ Microbiol* 84:e00354-18. <https://doi.org/10.1128/AEM.00354-18>.
- Schweiger P, Gross H, Deppenmeier U. 2010. Characterization of two aldo-keto reductases from *Gluconobacter oxydans* 621H capable of regio- and stereoselective alpha-ketocarbonyl reduction. *Appl Microbiol Biotechnol* 87:1415–1426. <https://doi.org/10.1007/s00253-010-2607-2>.
- Schiessl J, Kosciow K, Garschagen LS, Hoffmann JJ, Heymuth J, Franke T, Deppenmeier U. 2021. Degradation of the low-calorie sugar substitute 5-ketofructose by different bacteria. *Appl Microbiol Biotechnol* 105:2441–2453. <https://doi.org/10.1007/s00253-021-11168-3>.
- Chen R, Liu X, Lin J, Wei D. 2014. A genomic search approach to identify carbonyl reductases in *Gluconobacter oxydans* for enantioselective reduction of ketones. *Biosci Biotechnol Biochem* 78:1350–1356. <https://doi.org/10.1080/09168451.2014.925775>.
- Krajewski V, Simic P, Mouncey NJ, Bringer S, Sahn H, Bott M. 2010. Metabolic engineering of *Gluconobacter oxydans* for improved growth rate and growth yield on glucose by elimination of gluconate formation. *Appl Environ Microbiol* 76:4369–4376. <https://doi.org/10.1128/AEM.03022-09>.
- Yamada Y, Aida K, Uemura T. 1967. Enzymatic studies on the oxidation of sugar and sugar alcohol. II. Purification and properties of NADPH-linked 5-ketofructose reductase. *J Biochem* 61:803–811. <https://doi.org/10.1093/oxfordjournals.jbchem.a128616>.

23. Winn MD, Ballard CC, Cowtan KD, Dodson EJ, Emsley P, Evans PR, Keegan RM, Krissinel EB, Leslie AGW, McCoy A, McNicholas SJ, Murshudov GN, Pannu NS, Potterton EA, Powell HR, Read RJ, Vagin A, Wilson KS. 2011. Overview of the CCP4 suite and current developments. *Acta Crystallogr D Biol Crystallogr* 67:235–242. <https://doi.org/10.1107/S0907444910045749>.
24. Emsley P, Lohkamp B, Scott WG, Cowtan K. 2010. Features and development of Coot. *Acta Crystallogr D Biol Crystallogr* 66:486–501. <https://doi.org/10.1107/S0907444910007493>.
25. Krissinel E, Henrick K. 2007. Inference of macromolecular assemblies from crystalline state. *J Mol Biol* 372:774–797. <https://doi.org/10.1016/j.jmb.2007.05.022>.
26. Krissinel E, Henrick K. 2004. Secondary-structure matching (SSM), a new tool for fast protein structure alignment in three dimensions. *Acta Crystallogr D Biol Crystallogr* 60:2256–2268. <https://doi.org/10.1107/S0907444904026460>.
27. Lindner HA, Nadeau G, Matte A, Michel G, Menard R, Cygler M. 2005. Site-directed mutagenesis of the active site region in the quinate/shikimate 5-dehydrogenase YdiB of *Escherichia coli*. *J Biol Chem* 280:7162–7169. <https://doi.org/10.1074/jbc.M412028200>.
28. Peek J, Lee J, Hu S, Senisterra G, Christendat D. 2011. Structural and mechanistic analysis of a novel class of shikimate dehydrogenases: evidence for a conserved catalytic mechanism in the shikimate dehydrogenase family. *Biochemistry* 50:8616–8627. <https://doi.org/10.1021/bi200586y>.
29. Singh S, Stavrinides J, Christendat D, Guttman DS. 2008. A phylogenomic analysis of the shikimate dehydrogenases reveals broadscale functional diversification and identifies one functionally distinct subclass. *Mol Biol Evol* 25:2221–2232. <https://doi.org/10.1093/molbev/msn170>.
30. Peek J, Garcia C, Lee J, Christendat D. 2013. Insights into the function of RifI2: structural and biochemical investigation of a new shikimate dehydrogenase family protein. *Biochim Biophys Acta* 1834:516–523. <https://doi.org/10.1016/j.bbapap.2012.10.016>.
31. Singh S, Korolev S, Koroleva O, Zarembinski T, Collart F, Joachimiak A, Christendat D. 2005. Crystal structure of a novel shikimate dehydrogenase from *Haemophilus influenzae*. *J Biol Chem* 280:17101–17108. <https://doi.org/10.1074/jbc.M412753200>.
32. Kubota T, Tanaka Y, Hiraoka K, Inui M, Yukawa H. 2013. Characterization of shikimate dehydrogenase homologues of *Corynebacterium glutamicum*. *Appl Microbiol Biotechnol* 97:8139–8149. <https://doi.org/10.1007/s00253-012-4659-y>.
33. Höppner A, Schomburg D, Niefind K. 2013. Enzyme-substrate complexes of the quinate/shikimate dehydrogenase from *Corynebacterium glutamicum* enable new insights in substrate and cofactor binding, specificity, and discrimination. *Biol Chem* 394:1505–1516. <https://doi.org/10.1515/hsz-2013-0170>.
34. Michel G, Roszak AW, Sauvé V, Maclean J, Matte A, Coggins JR, Cygler M, Laphorn AJ. 2003. Structures of shikimate dehydrogenase AroE and its Paralog YdiB. A common structural framework for different activities. *J Biol Chem* 278:19463–19472. <https://doi.org/10.1074/jbc.M300794200>.
35. Adachi O, Ano Y, Toyama H, Matsushita K. 2006. Purification and properties of NADP-dependent shikimate dehydrogenase from *Gluconobacter oxydans* IFO 3244 and its application to enzymatic shikimate production. *Biosci Biotechnol Biochem* 70:2786–2789. <https://doi.org/10.1271/bbb.60305>.
36. Liu DF, Ai GM, Zheng QX, Liu C, Jiang CY, Liu LX, Zhang B, Liu YM, Yang C, Liu SJ. 2014. Metabolic flux responses to genetic modification for shikimic acid production by *Bacillus subtilis* strains. *Microb Cell Fact* 13:40. <https://doi.org/10.1186/1475-2859-13-40>.
37. Bagautdinov B, Kunishima N. 2007. Crystal structures of shikimate dehydrogenase AroE from *Thermus thermophilus* HB8 and its cofactor and substrate complexes: insights into the enzymatic mechanism. *J Mol Biol* 373:424–438. <https://doi.org/10.1016/j.jmb.2007.08.017>.
38. Schoepe J, Niefind K, Schomburg D. 2008. 1.6 angstroms structure of an NAD⁺-dependent quinate dehydrogenase from *Corynebacterium glutamicum*. *Acta Crystallogr D Biol Crystallogr* 64:803–809. <https://doi.org/10.1107/S090744490801411X>.
39. Peek J, Christendat D. 2015. The shikimate dehydrogenase family: functional diversity within a conserved structural and mechanistic framework. *Arch Biochem Biophys* 566:85–99. <https://doi.org/10.1016/j.abb.2014.12.006>.
40. Gan J, Wu Y, Prabakaran P, Gu Y, Li Y, Andrykovitch M, Liu H, Gong Y, Yan H, Ji X. 2007. Structural and biochemical analyses of shikimate dehydrogenase AroE from *Aquifex aeolicus*: implications for the catalytic mechanism. *Biochemistry* 46:9513–9522. <https://doi.org/10.1021/bi602601e>.
41. Schrimsher JL, Wingfield PT, Bernard A, Mattaliano R, Payton MA. 1988. Purification and characterization of 5-ketofructose reductase from *Erwinia citreus*. *Biochem J* 253:511–516. <https://doi.org/10.1042/bj2530511>.
42. Blanchard JS, Brewer CF, England S, Avigad G. 1982. Solution structure of 5-keto-D-fructose: relevance to the specificity of hexose kinases. *Biochemistry* 21:75–81. <https://doi.org/10.1021/bi00530a014>.
43. Siemen A, Kosciow K, Schweiger P, Deppenmeier U. 2018. Production of 5-ketofructose from fructose or sucrose using genetically modified *Gluconobacter oxydans* strains. *Appl Microbiol Biotechnol* 102:1699–1710. <https://doi.org/10.1007/s00253-017-8699-1>.
44. Adachi O, Ano Y, Toyama H, Matsushita K. 2006. Enzymatic preparation of metabolic intermediates, 3-dehydroquininate and 3-dehydroshikimate, in the shikimate pathway. *Biosci Biotechnol Biochem* 70:3081–3083. <https://doi.org/10.1271/bbb.60414>.
45. Hanahan D. 1983. Studies on transformation of *Escherichia coli* with plasmids. *J Mol Biol* 166:557–580. [https://doi.org/10.1016/s0022-2836\(83\)80284-8](https://doi.org/10.1016/s0022-2836(83)80284-8).
46. Studier FW, Moffatt BA. 1986. Use of bacteriophage T7 RNA polymerase to direct selective high-level expression of cloned genes. *J Mol Biol* 189:113–130. [https://doi.org/10.1016/0022-2836\(86\)90385-2](https://doi.org/10.1016/0022-2836(86)90385-2).
47. Studier FW. 1991. Use of bacteriophage T7 lysozyme to improve an inducible T7 expression system. *J Mol Biol* 219:37–44. [https://doi.org/10.1016/0022-2836\(91\)90855-z](https://doi.org/10.1016/0022-2836(91)90855-z).
48. Marmur J. 1961. A procedure for the isolation of deoxyribonucleic acid from micro-organisms. *J Mol Biol* 3:208–218. [https://doi.org/10.1016/S0022-2836\(61\)80047-8](https://doi.org/10.1016/S0022-2836(61)80047-8).
49. Yorimitsu T, Mimaki A, Yakushi T, Homma M. 2003. The conserved charged residues of the C-terminal region of FLiG, a rotor component of the Na⁺-driven flagellar motor. *J Mol Biol* 334:567–583. <https://doi.org/10.1016/j.jmb.2003.09.052>.
50. Kovach ME, Elzer PH, Hill DS, Robertson GT, Farris MA, Roop RM 2nd, Peterson KM. 1995. Four new derivatives of the broad-host-range cloning vector pBBR1MCS, carrying different antibiotic-resistance cassettes. *Gene* 166:175–176. [https://doi.org/10.1016/0378-1119\(95\)00584-1](https://doi.org/10.1016/0378-1119(95)00584-1).
51. Marx CJ, Lidstrom ME. 2001. Development of improved versatile broad-host-range vectors for use in methylotrophs and other Gram-negative bacteria. *Microbiology (Reading)* 147:2065–2075. <https://doi.org/10.1099/00221287-147-8-2065>.
52. Kostner D, Peters B, Mientus M, Liebl W, Ehrenreich A. 2013. Importance of *codB* for new *codA*-based markerless gene deletion in *Gluconobacter* strains. *Appl Microbiol Biotechnol* 97:8341–8349. <https://doi.org/10.1007/s00253-013-5164-7>.
53. Yakushi T, Terada Y, Ozaki S, Kataoka N, Akakabe Y, Adachi O, Matsutani M, Matsushita K. 2018. Aldopentoses as new substrates for the membrane-bound, pyrroloquinoline quinone-dependent glycerol (polyol) dehydrogenase of *Gluconobacter* sp. *Appl Microbiol Biotechnol* 102:3159–3171. <https://doi.org/10.1007/s00253-018-8848-1>.
54. Kabsch W. 2010. XDS. *Acta Crystallogr D Biol Crystallogr* 66:125–132. <https://doi.org/10.1107/S0907444909047337>.
55. Evans P. 2006. Scaling and assessment of data quality. *Acta Crystallogr D Biol Crystallogr* 62:72–82. <https://doi.org/10.1107/S0907444905036693>.
56. Evans PR. 2011. An introduction to data reduction: space-group determination, scaling and intensity statistics. *Acta Crystallogr D Biol Crystallogr* 67:282–292. <https://doi.org/10.1107/S090744491003982X>.
57. Vagin A, Teplyakov A. 1997. MOLREP: an automated program for molecular replacement. *J Appl Crystallogr* 30:1022–1025. <https://doi.org/10.1107/S0021889897006766>.
58. Padyana AK, Burley SK. 2003. Crystal structure of shikimate 5-dehydrogenase (SDH) bound to NADP: insights into function and evolution. *Structure* 11:1005–1013. [https://doi.org/10.1016/s0969-2126\(03\)00159-x](https://doi.org/10.1016/s0969-2126(03)00159-x).
59. Murshudov GN, Skubák P, Lebedev AA, Pannu NS, Steiner RA, Nicholls RA, Winn MD, Long F, Vagin AA. 2011. REFMAC5 for the refinement of macromolecular crystal structures. *Acta Crystallogr D Biol Crystallogr* 67:355–367. <https://doi.org/10.1107/S0907444911001314>.
60. McNicholas S, Potterton E, Wilson KS, Noble ME. 2011. Presenting your structures: the CCP4mg molecular-graphics software. *Acta Crystallogr D Biol Crystallogr* 67:386–394. <https://doi.org/10.1107/S0907444911007281>.
61. Schüttelkopf AW, van Aalten DM. 2004. PRODRG: a tool for high-throughput crystallography of protein-ligand complexes. *Acta Crystallogr D Biol Crystallogr* 60:1355–1363. <https://doi.org/10.1107/S0907444904011679>.
62. Altschul SF, Madden TL, Schaffer AA, Zhang J, Zhang Z, Miller W, Lipman DJ. 1997. Gapped BLAST and PSI-BLAST: a new generation of protein database search programs. *Nucleic Acids Res* 25:3389–3402. <https://doi.org/10.1093/nar/25.17.3389>.
63. Edgar RC. 2004. MUSCLE: multiple sequence alignment with high accuracy and high throughput. *Nucleic Acids Res* 32:1792–1797. <https://doi.org/10.1093/nar/gkh340>.
64. Edgar RC. 2004. MUSCLE: a multiple sequence alignment method with reduced time and space complexity. *BMC Bioinformatics* 5:113. <https://doi.org/10.1186/1471-2105-5-113>.

65. Tamura K, Dudley J, Nei M, Kumar S. 2007. MEGA4: Molecular Evolutionary Genetics Analysis (MEGA) software version 4.0. *Mol Biol Evol* 24:1596–1599. <https://doi.org/10.1093/molbev/msm092>.
66. Stecher G, Tamura K, Kumar S. 2020. Molecular Evolutionary Genetics Analysis (MEGA) for macOS. *Mol Biol Evol* 37:1237–1239. <https://doi.org/10.1093/molbev/msz312>.
67. Crooks GE, Hon G, Chandonia JM, Brenner SE. 2004. WebLogo: a sequence logo generator. *Genome Res* 14:1188–1190. <https://doi.org/10.1101/gr.849004>.
68. Adachi O, Toyama H, Matsushita K. 1999. Crystalline NADP-dependent D-mannitol dehydrogenase from *Gluconobacter suboxydans*. *Biosci Biotechnol Biochem* 63:402–407. <https://doi.org/10.1271/bbb.63.402>.
69. Zahid N, Deppenmeier U. 2016. Role of mannitol dehydrogenases in osmoprotection of *Gluconobacter oxydans*. *Appl Microbiol Biotechnol* 100:9967–9978. <https://doi.org/10.1007/s00253-016-7680-8>.
70. Benach J, Lee I, Edstrom W, Kuzin AP, Chiang Y, Acton TB, Montelione GT, Hunt JF. 2003. The 2.3-Å crystal structure of the shikimate 5-dehydrogenase orthologue YdiB from *Escherichia coli* suggests a novel catalytic environment for an NAD-dependent dehydrogenase. *J Biol Chem* 278:19176–19182. <https://doi.org/10.1074/jbc.M301348200>.
71. Stark MJ. 1987. Multicopy expression vectors carrying the *lac* repressor gene for regulated high-level expression of genes in *Escherichia coli*. *Gene* 51:255–267. [https://doi.org/10.1016/0378-1119\(87\)90314-3](https://doi.org/10.1016/0378-1119(87)90314-3).